Hybrid ARQ Throughput Performance of Multicode DS-CDMA MIMO Multiplexing

Akinori Nakajima[+] *and Fumiyuki Adachi*[++]

Dept. of Electrical and Communication Engineering, Graduate School of Engineering,
Tohoku University, Japan
E-mail: [+]nakajima@mobile.ecei.tohoku.ac.jp, [++]adachi@ecei.tohoku.ac.jp

Abstract— One of the promising techniques to allow high-speed data transmission with a limited bandwidth is multi-input multi-output (MIMO) multiplexing. As a signal separation scheme, an iterative frequency-domain interference cancellation (FD-IC) using two-dimensional minimum mean square error (2D-MMSE) frequency-domain equalization (FDE) was recently proposed. There are two types of FD-IC: parallel FD-IC (FD-PIC) and successive FD-IC (FD-SIC). Hybrid ARQ of multicode DS-CDMA MIMO multiplexing using FD-IC is considered in this paper. The achievable throughput performance is evaluated by computer simulation to show that FD-PIC is promising since FD-PIC is less computationally complex and has lower processing delay than FD-SIC.

Key words: *Hybrid ARQ, multicode DS-CDMA MIMO multiplexing, iterative FD-IC, mobile communication*

1. INTRODUCTION

In the next generation wireless systems, high-speed packet data services of e.g. 100M~1Gbps are demanded [1]. Using multicode DS-CDMA, flexible high-speed variable data transmission can be achieved while retaining the multi access capability. However, for such a high data rate transmission, the transmission performance significantly degrades due to severe inter-path interference (IPI) resulting from a severe frequency-selective channel [2]. Recently, it was shown [3,4] that frequency-domain equalization (FDE) can significantly improve the multicode DS-CDMA transmission performance. However, the available bandwidth is limited. One of the promising techniques to allow high-speed data transmission with a limited bandwidth is multi-input multi-output (MIMO) multiplexing [5], that uses multiple transmit and receive antennas.

Broadband wireless packet access will be the core technology of the next generation mobile communication systems. For very high-speed and high-quality packet transmissions in a limited bandwidth, the joint use of MIMO multiplexing and rate compatible punctured turbo coded-hybrid automatic repeat request (RCPT-HARQ) [6] is very effective. In this paper, we consider HARQ of multicode DS-CDMA MIMO multiplexing. A lot of research attention has been paid to the signal detection schemes with reduced complexity while providing a performance close to maximum likelihood detection (MLD) [2]. Recently, we proposed an iterative frequency-domain interference cancellation (FD-IC) using two-dimensional minimum mean square error (2D-MMSE) FDE for non-spread single-carrier (SC)-MIMO multiplexing [7,8]. There are two types of FD-IC: parallel FD-IC (FD-PIC) [7] and successive FD-IC (FD-SIC) [8]. In this paper, we apply iterative FD-IC using 2D-MMSE FDE to HARQ of multicode DS-CDMA MIMO multiplexing. The achievable throughput performance is evaluated by computer simulation.

The remainder of this paper is organized as follows. Section 2 describes the HARQ of multicode DS-CDMA MIMO multiplexing using iterative FD-IC. Section 3 presents the computer simulated HARQ throughput performance in a frequency-selective Rayleigh fading channel. Section 4 concludes this paper.

2. HARQ of multicode DS-CDMA MIMO multiplexing using iterative FD-IC

2.1. Transmission system

Fig.1 illustrates the transmitter/receiver structure of RCPT-HARQ of multicode DS-CDMA (N_t,N_r)MIMO multiplexing with iterative FD-IC using 2D-MMSE FDE. N_t and N_r denote the number of transmit antennas and that of receive antennas, respectively.

At the transmitter, RCPT encoding is performed first. In this paper, type II HARQ S-P2 [9] is considered. After data-modulation, the symbol sequence is serial-to-parallel (S/P) converted to N_t parallel symbol streams $\{d_{n_t}(n)\}$, n_t=0~N_t-1, and then multicode spreading using C orthogonal spreading codes with spreading factor SF is applied to each symbol stream. Each of the resulting N_t multicode chip streams is divided into a sequence $\{s_{n_t}(t)\}$ of blocks of N_c chips each. The last N_g chips in each block is copied and inserted as a cyclic prefix into the guard interval (GI) placed at the beginning of each N_c-chip block. N_t GI-inserted multicode chip-blocks are then transmitted simultaneously from N_t transmit antennas.

At the receiver, a superposition of N_t multicode chip-blocks is received by N_r antennas. After the removal of GI, N_c-point FFT is applied to decompose the received signal block into N_c frequency components. The kth frequency component $R_{n_r}(k)$ received on the n_rth antenna can be expressed as

$$R_{n_r}(k) = \sqrt{\frac{2E_c}{T_c}} \sum_{n_t=0}^{N_t-1} H_{n_r,n_t}(k) S_{n_t}(k) + \Pi_{n_r}(k), \quad (1)$$

where E_c is the chip energy, T_c is the chip length, $H_{n_r,n_t}(k)$ is the kth frequency complex channel gain between the n_tth transmit antenna and the n_rth receive antenna, $S_{n_t}(k)$ is the kth frequency component of the transmitted chip-block $\{s_{n_t}(t)\}$, and $\Pi_{n_r}(k)$ is the noise component associated with the n_rth receive antenna. $H_{n_r,n_t}(k)$, $S_{n_t}(k)$, and $\Pi_{n_r}(k)$ are given as

$$\begin{cases} H_{n_r,n_t}(k) = \sum_{l=0}^{L-1} h_{n_r,n_t,l} \exp\left(-j2\pi k \frac{\tau_l}{N_c}\right) \\ S_{n_t}(k) = \sum_{t=0}^{N_c-1} s_{n_t}(t) \exp\left(-j2\pi k \frac{t}{N_c}\right) \\ \Pi_{n_r}(k) = \sum_{t=0}^{N_c-1} n_{n_r}(t) \exp\left(-j2\pi k \frac{t}{N_c}\right) \end{cases}, \quad (2)$$

where $h_{n_r,n_t,l}$ denotes the lth path gain between the n_rth receive antenna and the n_tth transmit antenna and $n_{n_r}(t)$ is a zero-mean complex Gaussian process having variance $2N_0/T_c$ with N_0 being the one-sided power spectrum density of additive white Gaussian noise (AWGN). After performing FFT, the iterative FD-IC using 2D-MMSE FDE is carried out for the signal separation/detection, followed by IFFT, multicode de-spreading and LLR computation for RCPT decoding and error detection. The result of error detection is fedback to the transmitter as ACK/NACK.

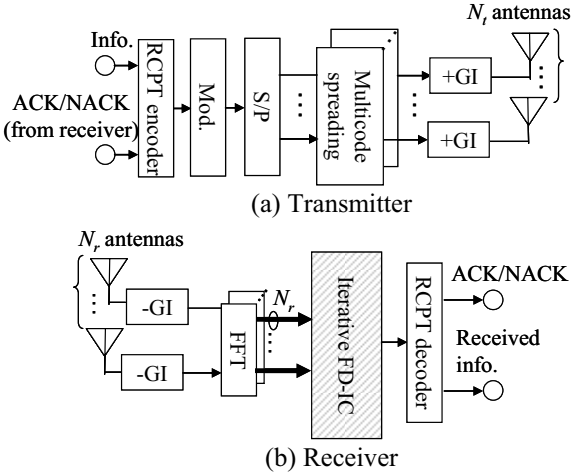

Figure 1 Transmitter/receiver structure.

2.2. Iterative FD-PIC

In FD-PIC, parallel signal separation/detection is performed. At first, 2D-MMSE FDE is performed. However, the interference can not be sufficiently suppressed. Therefore, FD-PIC using 2D-MMSE FDE is iterated a sufficient number of times. Fig.2 shows the flow chart of the iterative FD-PIC. Iterative FD-PIC consists of (a) FD-PIC, (b) 2D-MMSE FDE, (c) LLR computation and (c) replica generation. The ith iteration's operation is explained below.

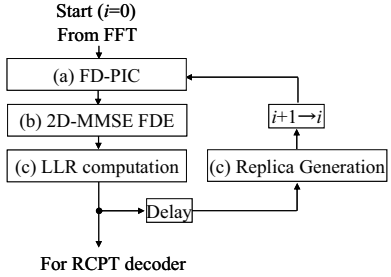

Figure 2 Iterative FD-PIC flow chart.

(a) FD-PIC

FD-PIC is performed to extract the frequency component $\hat{R}^{(i)}_{n_t,n_r}(k)$ of the chip-block transmitted from the n_tth antenna as

$$\hat{R}^{(i)}_{n_t,n_r}(k) = R_{n_r}(k) - \sqrt{\frac{2E_c}{T_c}} \sum_{\substack{n_t'=0 \\ \neq n_t}}^{N_t-1} H_{n_r,n_t'}(k) \hat{S}^{(i-1)}_{n_t'}(k), \quad (3)$$

where $\hat{S}^{(i-1)}_{n_t'}(k)$ is the replica of the n_t' th signal component generated based on the decision feedback from the (i-1)th iteration, $n_t' = 0 \sim N_t - 1$. However, at the first iteration (i=0), FD-PIC is not performed.

(b) 2D-MMSE FDE

After performing FD-PIC, 2D-MMSE FDE is carried out. The kth frequency component of the n_tth chip-block after 2D-MMSE FDE is denoted by $\tilde{R}^{(i)}_{n_t}(k)$ and is given as

$$\tilde{R}^{(i)}_{n_t}(k) = \mathbf{w}^{(i)}_{n_t}(k) \hat{\mathbf{R}}^{(i)}_{n_t}(k), \quad (4)$$

where $\hat{\mathbf{R}}^{(i)}_{n_t}(k) = [\hat{R}^{(i)}_{n_t,0}(k), \cdots, \hat{R}^{(i)}_{n_t,N_r-1}(k)]^T$ is the N_r-by-1 received signal vector after FD-PIC. $\mathbf{w}^{(i)}_{n_t}(k) = [w^{(i)}_{0,n_t}(k), \cdots, w^{(i)}_{N_r-1,n_t}(k)]$ is the 1-by-N_r 2D-MMSE weight vector. $\mathbf{w}^{(i)}_{n_t}(k)$ is given as

$$\mathbf{w}^{(i)}_{n_t}(k) = \mathbf{H}^H_{n_t}(k) \left[\mathbf{H}(k) \mathbf{G}^{(i)}_{n_t} \mathbf{H}^H(k) + \left(\frac{C \cdot E_c}{N_0} \right)^{-1} \mathbf{I} \right]^{-1}, \quad (5)$$

where $(.)^H$ is the Hermitian transpose operation, $\mathbf{I}$ is the N_r-by-N_r identity matrix and $\mathbf{H}_{n_t}(k) = [H_{0,n_t}(k), \cdots, H_{N_r-1,n_t}(k)]^T$ is N_r-by-1 channel gain vector. E_c/N_0 represents the average received chip energy-to-AWGN power spectrum density ratio per receive antenna and C is the code-multiplexing order. $\mathbf{G}^{(i)}_{n_t} = diag[g^{(i)}_{n_t,0}, \cdots, g^{(i)}_{n_t,N_t-1}]$ is an N_t-by-N_t matrix,

where $g_{n_t,n_t'}^{(i)}$ reflects the contribution of interference from the n_t'th antenna. $g_{n_t,n_t'}^{(i)}$ is given by

$$g_{n_t,n_t'}^{(i)} = \begin{cases} 1, & \text{if } n_t' = n_t \\ \dfrac{SF}{C \cdot N_c} \displaystyle\sum_{n=0}^{\frac{C \cdot N_c}{SF}-1} \left\{ \begin{matrix} |\, \tilde{d}_{n_t'}^{(i-1)}(n)\,|^2 \\ -|\, \hat{d}_{n_t'}^{(i-1)}(n)\,|^2 \end{matrix} \right\}, & \text{otherwise} \end{cases}, \quad (6)$$

where $\{\hat{d}_{n_t'}^{(i-1)}(n); n = 0 \sim (C \cdot N_c / SF) - 1\}$ is the soft replica of the symbol sequence $\{d_{n_t'}(n)\}$ in a chip-block transmitted from the n_t' th antenna, $\{\tilde{d}_{n_t'}^{(i-1)}(n); n = 0 \sim (C \cdot N_c / SF) - 1\}$ is the hard replica of $\{d_{n_t'}(n)\}$, and $g_{n_t,n_t'}^{(i=0)} = 1$. $\{\tilde{d}_{n_t'}^{(i-1)}(n)\}$ and $\{\hat{d}_{n_t'}^{(i-1)}(n)\}$ are generated based on the decision feedback from the (*i*-1)th iteration.

(c) LLR computation and replica generation

The time-domain received chip-block $\{\tilde{s}_{n_t}^{(i)}(t)$; t=0~N_c-1$\}$ is obtained by performing N_c-point IFFT on $\{\tilde{R}_{n_t}^{(i)}(k)$; k=0~N_c-1$\}$ after carrying out 2D-MMSE FDE in the ith iteration. Then, de-scrambling and multicode de-spreading operation yield the decision variable $\tilde{d}_{n_t}^{(i)}(n)$ of the nth symbol transmitted from the n_tth antenna.

The log likelihood ratio (LLR), $\lambda_{n_t}^{(i)}(m;n)$, of the mth bit $b_{n_t}(m;n)$ in the nth symbol transmitted from the n_tth transmit antenna is computed using $\tilde{d}_{n_t}^{(i)}(n)$ as [10]

$$\lambda_{n_t}^{(i)}(m;n) \approx \frac{1}{2\bar{\sigma}_{n_t}^{(i)^2}} \left(\left| \tilde{d}_{n_t}^{(i)}(n) - \sqrt{\frac{2E_c}{T_c}} \hat{H}_{n_t}^{(i)} \bar{d}_{b_{n_t}(m;n)=0}^{\min} \right|^2 - \left| \tilde{d}_{n_t}^{(i)}(n) - \sqrt{\frac{2E_c}{T_c}} \hat{H}_{n_t}^{(i)} \bar{d}_{b_{n_t}(m;n)=1}^{\min} \right|^2 \right), \quad (7)$$

where $\hat{H}_{n_t}^{(i)}$ is the equivalent channel gain of the n_tth transmit antenna at the ith iteration and is given by

$$\hat{H}_{n_t}^{(i)} = \frac{1}{N_c} \sum_{k=0}^{N_c-1} \mathbf{w}_{n_t}^{(i)}(k) \mathbf{H}_{n_t}(k). \quad (8)$$

$\bar{d}_{b_{n_t}(m;n)=0}^{\min}$ ($\bar{d}_{b_{n_t}(m;n)=1}^{\min}$) is the most probable symbol whose mth bit is 0 (or 1), for which the Euclidean distance from $\tilde{d}_{n_t}^{(i)}(n)$ is minimum. $2\bar{\sigma}_{n_t}^{(i)^2}$ is the variance of the IPI, the interference from other antennas plus noise and is given by

$$2\bar{\sigma}_{n_t}^{(i)^2} = \frac{2E_c}{SF \cdot T_c} \left[\begin{matrix} \left\{ \dfrac{1}{N_c} \displaystyle\sum_{k=0}^{N_c-1} \left| \mathbf{w}_{n_t}^{(i)}(k) \mathbf{H}_{n_t}(k) \right|^2 \right\} - \left| \hat{H}_{n_t} \right|^2 \\ + \left\{ \dfrac{1}{N_c} \displaystyle\sum_{\substack{n_t'=0 \\ \neq n_t}}^{N_t-1} g_{n_t,n_t'}^{(i)} \sum_{k=0}^{N_c-1} \left| \mathbf{w}_{n_t}^{(i)}(k) \mathbf{H}_{n_t'}(k) \right|^2 \right\} \\ + \left(\dfrac{E_c}{N_0} \right)^{-1} \dfrac{1}{N_c} \displaystyle\sum_{k=0}^{N_c-1} \sum_{n_r=0}^{N_r-1} |\, w_{n_r,n_t}^{(i)}(k)\,|^2 \end{matrix} \right]. \quad (9)$$

The soft replicas $\{\hat{d}_{n_t}^{(i)}(n)\}$, to be used for the next detection, are generated by using $\{\lambda_{n_t}^{(i)}(m;n)\}$ [7]. Multicode spreading and scrambling are performed on $\{\hat{d}_{n_t}^{(i)}(n)\}$ to obtain the multicode signal replica $\{\hat{s}_{n_t}^{(i)}(t)\}$. N_c-point FFT is performed on $\{\hat{s}_{n_t}^{(i)}(t)$; n_t=0~N_t-1$\}$ to obtain the frequency-domain signal replica $\{\hat{S}_{n_t}^{(i)}(k)$; k=0~N_c-1$\}$.

2.3. Iterative FD-SIC

The signal detection/cancellation is successively performed according to the descending order of the signals' reliability. Fig.3 shows the flow chart of the iterative FD-PIC. Iterative FD-SIC consists of (a) ordering, (b) FD-SIC, (c) 2D-MMSE FDE, (d) LLR computation and (d) replica generation. LLR computation and replica generation have already been explained in Sect. 2.2. The ith iteration's operation for the detection of the n_tth chip-block is explained below.

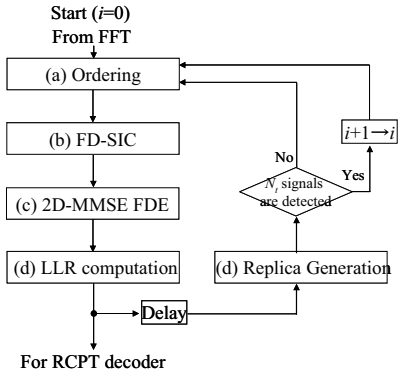

Figure 3 Iterative FD-SIC flow chart.

(a) Ordering

Without loss of generality, the transmit antenna having the highest equivalent channel gain is assumed to be the 0th transmit antenna, followed by the 1st, 2nd, …, (N_t-1)th antennas. The signal detection is performed for the signal which has the highest equivalent channel gain $\hat{H}_{n_t}^{(i)}$ among the undetected signals. $\hat{H}_{n_t}^{(i)}$ is computed by using Eq.(8). Until all the transmitted signals are detected, ordering is carried out at every signal detection.

(b) FD-SIC

Since the chip-blocks with $n_t' < n_t$ have already been detected, their replicas are generated using the decision feedback from the present ith iteration (i.e., $\hat{S}_{n_t'}^{(i)}(k)$ for $n_t' < n_t$). However, the chip-blocks with $n_t' > n_t$ are undetected and hence, their replicas are generated using the decision feedback from the (i-1)th iteration (i.e., $\hat{S}_{n_t'}^{(i-1)}(k)$ for $n_t' > n_t$). The frequency component $\hat{R}_{n_t,n_r}^{(i)}(k)$ of the chip-block transmitted from the n_tth antenna is extracted as

$$\hat{R}_{n_t,n_r}^{(i)}(k) = R_{n_r}(k) - \sqrt{\frac{2E_c}{T_c}} \left\{ \begin{array}{l} \displaystyle\sum_{n_t'=0}^{n_t-1} H_{n_r,n_t'}(k)\hat{S}_{n_t'}^{(i)}(k) \\ \displaystyle + \sum_{n_t'=n_t+1}^{N_t-1} H_{n_r,n_t'}(k)\hat{S}_{n_t'}^{(i-1)}(k) \end{array} \right\}. \quad (10)$$

(c) 2D-MMSE FDE

After performing FD-SIC, 2D-MMSE FDE is carried out by using Eqs. (4) and (5) with

$$g_{n_t,n_t'}^{(i)} = \begin{cases} \dfrac{SF}{C \cdot N_c} \displaystyle\sum_{n=0}^{\frac{C \cdot N_c}{SF}-1} \left\{ \begin{array}{l} |\breve{d}_{n_t'}^{(i)}(n)|^2 \\ -|\hat{d}_{n_t'}^{(i)}(n)|^2 \end{array} \right\}, & \text{if } n_t' < n_t \\ 1, & \text{if } n_t' = n_t \\ \dfrac{SF}{C \cdot N_c} \displaystyle\sum_{n=0}^{\frac{C \cdot N_c}{SF}-1} \left\{ \begin{array}{l} |\breve{d}_{n_t'}^{(i-1)}(n)|^2 \\ -|\hat{d}_{n_t'}^{(i-1)}(n)|^2 \end{array} \right\}, & \text{if } n_t' > n_t \end{cases} \quad (11)$$

Then, the detection of the (n_t+1)th chip-block is performed. After all the transmitted chip-blocks are detected, the next iteration is carried out.

3. Computer simulation

The computer simulation conditions are summarized in Table 1. We assume an information bit sequence of K=2048 bits. Coding rate R=1/3 turbo encoder, consisting of two (13,15) recursive systematic convolutional (RSC) encoders, is employed. In this paper, type II HARQ S-P2 [9] is considered. We assume $N_t \times N_r$ independent frequency-selective block Rayleigh fading channels, each channel has a chip-spaced exponentially decaying L=16-path power delay profile with decay factor αdB. The transmit chip-block length is N_c=256 chips and the GI length is N_g=32 chips. Ideal channel estimation is assumed.

The HARQ throughput performance for multicode DS-CDMA (4,4)MIMO multiplexing is plotted in Fig.4 as a function of the average received energy per symbol-to-AWGN power spectrum density ratio E_s/N_0 per receive antenna. The equivalent spreading factor SF_{eq} (=SF/C) is set as 1 (i.e., the transmission data rate is the same as non-spread SC). Since it was found that the use of four iterations (i=4) is enough to obtain a sufficient throughput improvement, only the throughput curves obtained with four iterations have been plotted.

Table 1. Simulation conditions

Transmitter	Data modulation	QPSK, 16QAM
	Number of Tx antennas	N_t=4
	Number of FFT points	N_c=256
	GI	N_g=32
Channel	Frequency-selective block Rayleigh fading	
	Power delay profile	L=16-path exponential
	Decay factor	α=0,6dB
Receiver	Number of Rx antennas	N_r=4
	Channel estimation	Ideal

First, we will discuss the impact of SF. It can be seen from Fig.4 that when α=0dB (strong selectivity), the throughput performance is insensitive to SF and close to that with perfect FD-IC (perfect cancellation of interference from other antennas) for both FD-PIC and FD-SIC. However, when α=6dB (weak selectivity), the performance dependency on SF is stronger and furthermore, the performance degradation from perfect FD-IC is lager than when α=0dB. This is because the accuracy of interference replica generation degrades since the channel gains at many frequencies fade simultaneously. However, as SF increases, the interference can be sufficiently suppressed and hence the throughput performance approaches that with perfect FD-IC.

Fig.5 compares FD-PIC and FD-SIC when SF=256. In general, SIC provides better transmission performance than PIC. As expected, the performance with FD-SIC is better than that with FD-PIC when both QPSK and 16QAM are used; however, the throughput difference between FD-PIC and FD-SIC is small. When QPSK is used, FD-PIC provides almost the same throughput performance as FD-SIC irrespective of α. On the other hand, when 16QAM is used, the loss in the required E_s/N_0 is only about 0.6dB and 0.4dB in the case of α=0dB and 6dB, respectively.

Next, we will discuss the complexity and the processing delay. The number of complex multiply operations required in FFT/IFFT operation and matrix inversion operation for PIC (i=4) is about 5 times less than for FD-SIC (i=4). Furthermore, the processing delay for FD-PIC is about N_t times less than FD-SIC. Therefore, FD-PIC requires much lower computational complexity and processing delay. Therefore, it can be said that FD-PIC is promising for HARQ of multicode DS-CDMA MIMO multiplexing.

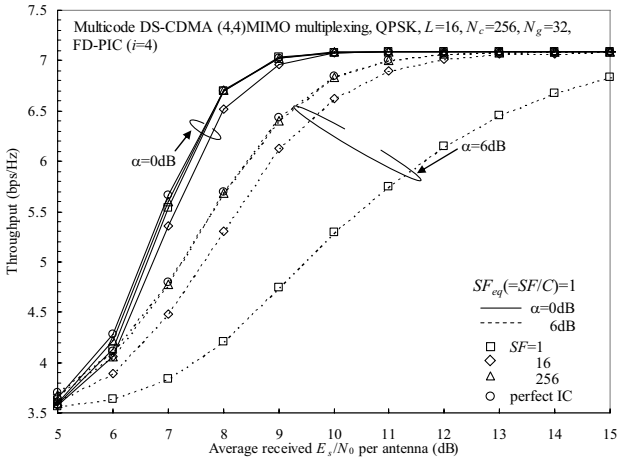

(a) FD-PIC

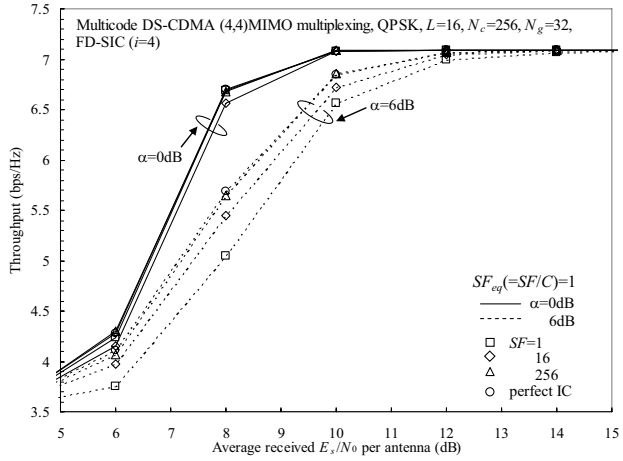

(b) FD-SIC

Figure 4 Impact of SF with SF/C=1.

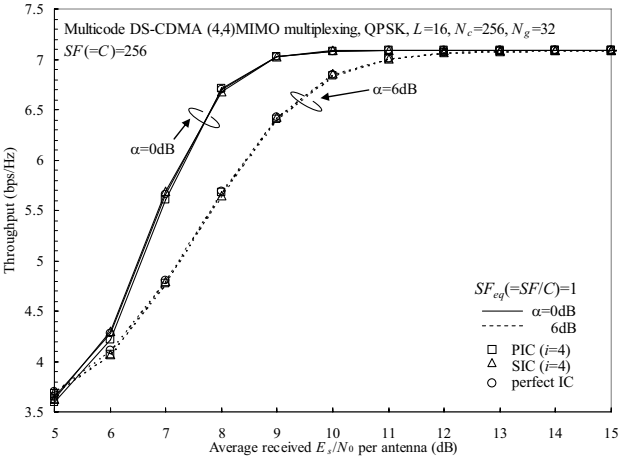

(a) QPSK

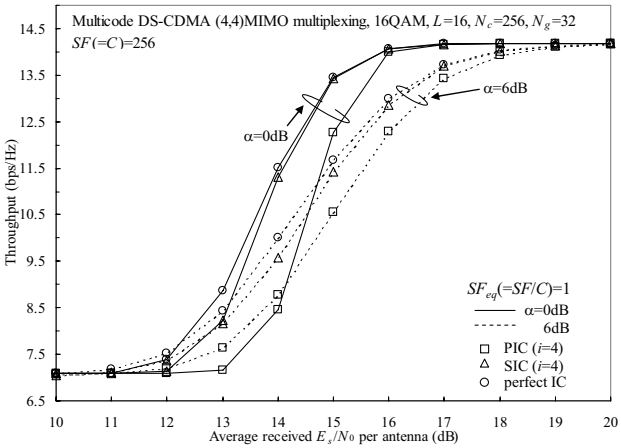

(b) 16QAM

Figure 5 Comparison of FD-SIC and FD-PIC.

4. CONCLUSIONS

In this paper, we evaluated the HARQ throughput performance of multicode DS-CDMA MIMO multiplexing using iterative FD-IC in a frequency-selective Rayleigh fading channel. It was shown that FD-PIC can achieve throughput only slightly lower than FD-SIC. Since FD-PIC is less computationally complex and has lower processing delay, FD-PIC is promising.

REFERENCES

[1] F. Adachi, "Wireless past and future-evolving mobile communications systems," IEICE Trans. Fundamentals, vol.E84-A, pp.55-60, Jan. 2001.

[2] John G. Proakis, *Digital Communications*, 4th edition, McGraw-Hill, 2001.

[3] D. Falconer, S. L. Ariyavisitakul, A. Benyamin-Seeyar, and B. Edison, "Frequency domain equalization for single-carrier broadband wireless systems," IEEE Commun. Mag., vol.40, pp.58-66, April 2002.

[4] F. Adachi, D. Garg, S. Takaoka, and K. Takeda, "Broadband CDMA techniques," IEEE Wireless Commun. Mag., Vol. 12, No. 2, pp. 8-18, April 2005.

[5] J. Hagenauer, "Rate-compatible punctured convolutional codes (RCPC codes) and their application," IEEE Trans. Commun., vol. 36, no. 4, pp.389-400, April 1988.

[6] G. J. Foschini and M. J. Gans, "On limits of wireless communications in a fading environment when using multiple antennas," Wireless Personal Commun., vol.6, No. 3, pp. 311-335, 1998.

[7] A. Nakajima and F. Adachi, "Iterative PIC using 2D MMSE-FDE for Turbo-coded HARQ with SC-MIMO Multiplexing," Proc. IEEE 63nd VTC, Melbourne, Australia., 7-10 May. 2006.

[8] A. Nakajima and F. Adachi, "Throughput Performance of Iterative Frequency-domain SIC with 2D MMSE-FDE for SC-MIMO Multiplexing," Proc. IEEE 64nd VTC, Montreal, Canada, Sept. 2006. (accepted)

[9] D. Garg and F. Adachi, "Throughput comparison of turbo-coded HARQ in OFDM, MC-CDMA and DS-CDMA with frequency-domain equalization," IEICE Trans. Commun., Vol. E88-B, No. 2, pp. 664-677, Feb. 2005.

[10] A. Stefanov and T. M. Duman, "Turbo coded modulation for wireless communications with antenna diversity," J. Commun. Netw., vol. 2, no. 4, pp. 356-360, Dec. 2000.

